Functional characterization of the Co^{2+} transporter AitP in *Sinorhizobium meliloti*: a new player in Fe^{2+} homeostasis

RUNNING TITLE: AitP Fe-export orchestrates the [Fe-S] salvage pathway

Paula Mihelj[1], Isidro Abreu[2*], Tomás Moreyra[1], Manuel González-Guerrero[2 3], Daniel Raimunda[1]

[1]Instituto de Investigación Médica Mercedes y Martín Ferreyra - INIMEC - CONICET, UNC. Córdoba, Argentina. [2]Centro de Biotecnología y Genómica de Plantas (UPM-INIA/CSIC), Universidad Politécnica de Madrid, Madrid, Spain. [3]Departamento de Biotecnología-Biología Vegetal. Escuela Técnica Superior de Ingeniería Agronómica, Alimentaria y de Biosistemas, Universidad Politécnica de Madrid, Madrid, Spain. *Current address: Department of Biology, University of Oxford, Oxford, UK.

Abstract

Co^{2+} induces the increase of the labile-Fe pool (LIP) by Fe-S cluster damage, heme synthesis inhibition and "free" iron import, which affects cell viability. The N_2-fixing bacteria, *Sinorhizobium meliloti,* is a suitable model to determine the roles of Co^{2+}-transporting Cation diffusion facilitator exporters (Co-eCDF) in Fe^{2+} homeostasis because it has a putative member of this sub-family, AitP, and two specific Fe^{2+}-export systems. An insertional mutant of AitP showed Co^{2+} sensitivity and accumulation, Fe accumulation and hydrogen peroxide sensitivity, but not Fe^{2+} sensitivity, despite AitP being a *bona fide* low affinity Fe^{2+} exporter as demonstrated by the kinetic analyses of Fe^{2+} uptake into everted membrane vesicles. Suggesting concomitant Fe^{2+}-dependent induced stress, Co^{2+} sensitivity was increased in strains carrying mutations in AitP and Fe^{2+} exporters which did not correlate with the Co^{2+} accumulation. Growth in the presence of sub-lethal Fe^{2+} and Co^{2+} concentrations suggested that free Fe-import might contribute to Co^{2+} toxicity. Supporting this, Co^{2+} induced transcription of Fe-import system and genes associated with Fe homeostasis. Analyses of total protoporphyrin content indicates Fe-S cluster attack as the major source for LIP. AitP-mediated Fe^{2+}-export is likely counterbalanced via a non-futile Fe^{2+}-import pathway. Two lines of evidence support this: i) an increased hemin uptake in presence of Co^{2+} was observed in WT *vs.* AitP mutant, and ii) hemin reversed the Co^{2+} sensitivity in the AitP mutant. Thus, the simultaneous detoxification mediated by AitP aids cells to orchestrate an Fe-S cluster salvage response, avoiding the increase in the LIP caused by the disassembly of Fe-S clusters or free iron uptake.

Importance

Cross-talk between iron and cobalt has been long recognized in biological systems. This is due to the capacity of cobalt to interfere with proper iron utilization. Cells can detoxify cobalt by exporting mechanisms involving membrane proteins known as exporters. Highlighting the cross-talk, the capacity of several cobalt exporters to also export iron is emerging. Although biologically less important than Fe^{2+}, Co^{2+} induces toxicity by promoting intracellular Fe release, which ultimately causes additional toxic effects. In this work, we describe how the N_2-fixating rhizobial cells solve this perturbation by clearing Fe through a Co^{2+}-exporter, in order to reestablish intracellular Fe-levels by importing non-free Fe, heme. This piggyback-ride type of transport may aid bacterial cells to survive in free-living conditions where high anthropogenic Co^{2+} content may be encountered.

43 **Introduction**

44 Cobalt (Co) and iron (Fe) are essential micronutrients in bacteria. While Fe is broadly
45 required to deal with biological reactions in the actual conditions ruled by dioxygen, Co is
46 involved in a handful of metabolic pathways as a catalytic cofactor or as the coenzyme
47 vitamin B_{12} [1-3]. The chemical properties of both Fe and Co mean that they become toxic
48 under certain conditions that promote increased bioavailability, i.e., high concentration in the
49 extracellular environment, or in the case of Fe, an increase in the exchange between
50 intracellular storage and the labile pool (*en route exchange*) [4, 5]. Although Fe toxicity
51 seems to be curbed by Fe-storage systems, recent studies have suggested that Fe
52 accumulation may exceed their buffering capacity and lead to redox stress [6, 7].

53 The rhizobial α-proteobacteria and alfalfa symbiont, *Sinorhizobium melliloti*, is involved in
54 biological N_2-fixation, a process highly dependent on Fe [8]. Previous studies describing
55 genetic and mechanistic findings on Fe acquisition, export and storage in α-protobacteria,
56 including rhizobia [9], share one of the two transcriptional factors, *irr* [10] and *rirA* [11], which
57 sense cellular Fe status through heme or Fe-S clusters, respectively. RirA regulates iron
58 uptake gene transcription, promoting free (ferric) and non-free (siderophore-iron complexes
59 or heme) iron uptake in low Fe conditions. Irr regulates genes involved in heme synthesis
60 and Fe exporters, derepressing their transcription in high Fe conditions. In *Agrobacterium*
61 *tumefaciens* and *Bradyrhizobium japonicum*, the membrane-bound ferritin A (MbfA), a
62 member of the CCC1 Fe efflux family, has been described to be involved in Fe homeostasis
63 [12, 13] . In *S. meliloti*, a P-type-IB-ATPase (Nia) has also been described as being specific
64 for Fe transport and upregulated under low O_2 conditions [14]. Cobalt is an essential nutrient
65 for *S. meliloti* and other rhizobia [15], and an uptake system has been identified in this
66 organism [16]. Similarly, the *dmeRF* system, consisting of a member of the FrmR family of
67 transcriptional regulators (DmeR) and a member of the cation diffusion facilitator (DmeF),

68 has been involved in Co^{2+} homeostasis through export, specifically during free-living stages
69 previous to establishing symbiosis and nodulation [17-19].

70 A feature of Co^{2+} dyshomeostasis is related to Fe-S cluster stability. There is evidence that
71 a high Co^{2+} condition induces Fe-S cluster disassembly, triggering *suf* and *isc* machinery in
72 response to this injury [20, 21]. The mechanisms proposed leading to Fe-S disruption by
73 Co^{2+} or other transition metals vary from the non-cognate metal interfering with assembly
74 process [20], to the Fe-S centers attacked in enzymes [22]. However, the final outcome in
75 order to supply Fe for cluster reconstitution relies on changes in the dynamic between
76 intracellular Fe stores and the labile-Fe pool (LIP) [23], and most importantly, the triggering
77 of free and non-free Fe uptake mechanisms [18, 21, 24].

78 In rhizobia, the Fe-S cluster synthesis pathway is regulated by the transcription factor RirA,
79 which represses the *suf* operon, the unique system for Fe-S cluster assembly in *S. meliloti*
80 [9], under replete Fe conditions [11]. RirA is a functional analog of Fur, the canonical Fe-
81 responsive transcriptional regulator, but differs from this in that it senses Fe indirectly
82 through an Fe-S cluster with a labile Fe as a proxy [25, 26]. Thus, under low iron conditions,
83 the release of RirA from the promoter region (IRO box) activates the transcription of the
84 genes in its regulon. *S. meliloti* presents a second transcriptional regulator, Irr, which senses
85 Fe status through heme binding and regulates *rirA* transcription, reinforcing the role of *rirA*
86 under low iron conditions [4].

87 Some authors have proposed a link between Co^{2+} and Fe^{2+} homeostasis, providing evidence
88 of a RirA-mediated response upon high extracellular Co^{2+}, involving upregulation of heme
89 uptake systems, probably as a result of an increase in the inactive apo form [18]. As a Co^{2+}
90 Fe-S cluster attack could lead to an increase in Fe^{2+} bioavailability [27-29], an Irr-mediated
91 response is also expected.

92 Importantly, previously described Co^{2+} transporters are emerging as Fe-exporters in
93 bacterial organisms [7, 30, 31]. Therefore, we decided to evaluate the Fe transport capacity
94 of SMc04167/AitP, a DmeF homolog in *S. meliloti*. Our data, showing that Co^{2+} induces Fe
95 dyshomeostasis by likely affecting dynamics in the LIP, and that Co^{2+} sensitivity can be
96 rescued in a non-competitive fashion by heme, together with the observations that AitP
97 exports Fe^{2+}, indicates a role for the FrmR/DmeR-regulated Co^{2+} exporters of the CDF family
98 at initial stages of the Co^{2+} induced mediated Fe-S cluster salvage pathway through Fe^{2+}
99 export.

100 **Results**

101 *AitP is a classical CDF Co^{2+} exporter member of a sub-family with non-unique operon*
102 *architectures*

103 A survey of more than 17,000 complete bacterial genomes allowed us to identify by Best-
104 Reciprocal-Hit more than 759 *dmeF*/*aitP*-like genes (Fig. 1A), showing typical features of
105 this Co^{2+} CDF subfamily. A multigene blast analysis showed that approximately 62% of
106 these share the archetypical operon organization of juxtaposed *frmR-aitP*/*dmeR-dmeF* loci
107 (Fig. 1A). The remaining percentage appears to have an FrmR-independent regulation with
108 no archetypical operon configuration and no operator-promoter region for the Co^{2+}
109 responsive transcriptional regulator FrmR/DmeR (Suppl. Table 1). These findings also
110 suggest that a significant number of putative Co^{2+} exporter *aitP*-like genes might be part of
111 Co^{2+}-responsive operons, with effectors other than Co^{2+} generated when this is
112 accumulated. Moreover, AitP-like members found in Co^{2+}-unresponsive operons could have
113 a broaden specificity of transport.

114 The genome of *S. meliloti* encodes a single member of the Co^{2+} efflux CDF subfamily
115 (SMc04167, AitP), a homolog of the DmeF protein described in *R. leguminosarum* [17], and
116 also of the AitP transporter of *Pseudomonas aeruginosa* [7]. As in other rhizobia, AitP is

117 preceded by a transcriptional regulator of the FrmR/DmeR family. Phenotypic analysis of
118 the insertional mutant of the SMc04167 locus in *S. meliloti* Rm1021 (Ω04167 or "AitP
119 mutant") shows increased Co^{2+} sensitivity in this strain (Fig. 1B). The sensitivity was
120 concentration-dependent and it was rescued after gene complementation (Fig. 1C-D). Co^{2+}
121 and Fe^{2+} accumulation occurred in the Ω04167 strain after incubation for 1 hour with 0.2 mM
122 Co^{2+} or 20 minutes with 1.5 mM Fe^{2+},and complementation of Ω04167 reverted the
123 accumulation to WT levels (Fig. 1E). Cell numbers after incubation were the same in all
124 strains, indicating that these treatments (time and Co^{2+} or Fe^{2+} concentrations) are sub-lethal
125 (not shown). Although the Fe^{2+} accumulation in AitP mutant did not induce a defect in cell
126 growth, the double mutant lacking AitP and MbfA transporters was more sensitive to
127 hydrogen peroxide (H_2O_2) than the MbfA single mutant in growth media with no external Fe
128 added (Fig.1F). Free Fe^{2+} catalyzes the formation of reactive oxygen species through a
129 Fenton reaction, which indicates that AitP functions as an Fe^{2+} exporter. As expected,
130 transcription of *aitP* and *frmR*/*dmeR* was upregulated by Co^{2+}(Fig. 1G) but was
131 unresponsive to Fe^{2+} in the case of *aitP* as opposed to *mbfA* (Fig. 1H).

132 *AitP shows a dual specificity of transport*

133 The phenotypical findings (Fig. 1E-F) agree with previous studies on AitP-like members [7],
134 but suggest an alternative role in Fe^{2+} export by AitP. As Fe^{2+} homeostasis plays a significant
135 role for the rhizobia-legume symbiosis, we decided to test whether Fe^{2+} could be transported
136 by AitP. This could be hindered by the apparently redundant *mbfA* and *nia* Fe^{2+} transport
137 systems [12-14]. Therefore, we heterologously overexpressed AitP in the Δ*fieF E. coli* strain
138 (Suppl. Fig. 1A). FieF was previously described as an Fe^{2+} transporter [31, 32], and thus the
139 genotypic background lacking FieF would allow measurement of Fe^{2+} with a low background
140 signal. After protein induction, everted membrane vesicles were obtained and energized by
141 pre-incubation with the electron donor NADH (or lactate), generating a H^+-electrochemical

142 gradient (Suppl. Fig. 1B). Only in this condition was $^{59}Fe^{2+}$-importing activity to the vesicle
143 detected, indicating that Fe^{2+} is a substrate transported by AitP, and that the driving force is
144 the electrochemical gradient of H^+ (Fig. 2A). After initial rate conditions were determined, we
145 characterized the kinetics of the transport (Fig 2B). The estimated $K_{1/2}$ value at the low
146 millimolar range (1.35±0.21) may indicate a low affinity for transport, in line with the iron-
147 saving strategies observed in almost all living organisms toward intracellular Fe^{2+}. The H^+-
148 dependent transport at sub-saturating concentrations (Fe^{2+} = 2mM) was inhibited only by
149 Co^{2+}, indicating that competition at the transport site is possible (Fig. 2C). However, Co^{2+}
150 accumulation observed in the AitP mutant (Fig. 1E) suggests a dual (Fe/Co) transport
151 specificity, with both ions as cytosolic substrates, likely exported by a sequential mechanism
152 involving binding to the same transport site. Considering the absence of Fe^{2+} regulation in
153 *aitP* transcription, these results suggest a role for AitP in Fe^{2+} transport in conditions in which
154 concomitant intracellular Co^{2+} accumulation occurs.

155 *AitP participates in Fe-homeostasis*

156 Previous phenotypical characterizations of *aitP*-like genes in other rhizobial organisms point
157 to a similar role of AitP in Co^{2+} export and detoxification [17-19], and we have previously
158 shown that the AitP homolog in *P. aeruginosa* is involved in Fe^{2+} homeostasis [7]. However,
159 a P-IB-type ATPase, *nia*, has been described as participating in Fe^{2+} homeostasis in this
160 organism [14], and the identification of an *mbfA* ortholog in Rm1021 genome led us to
161 hypothesize that AitP in *S. meliloti* may play a non-classical role in Fe^{2+} homeostasis. In this
162 line, Fe^{2+} sensitivity was not observed in the Ω04167 strain, pointing to *nia* and *mbfA* as
163 major exit routes for Fe^{2+} in rhizobia. As Co^{2+} transport has been described through Fe^{2+}
164 exporters, we conducted phenotypical analyses to test whether double mutants showed
165 increased sensitivity towards Co^{2+}. We observed an increased sensitivity in the double
166 mutants, Ω3004 and Ω03808, beyond the threshold shown by the Ω04167 strain (Fig. 3A)

167 but, interestingly, no significant increases of Co^{2+} accumulation were observed *vs*. the
168 Ω04167 strain (Fig. 3B). Supporting the exclusive participation of AitP in Co^{2+} efflux, Co^{2+}-
169 dependent *nia* transcription is not expected [14], and *mbfA* was not induced by Co^{2+} (Fig.
170 1G). Thus, we hypothesized a possible Fe^{2+}-induced toxic effect being added to those
171 promoted by Co^{2+} accumulation. To test this, we measured the Co^{2+} sensitivity of the
172 Ω04167 *vs*. Rm1021 in the presence of Fe. The increased sensitivity shown by Ω04167 in
173 this condition (Fig. 3C) indicates that Co^{2+} accumulation induces a shift in iron distribution,
174 with increased LIP or higher levels of Fe^{2+} bioavailability that result toxic to the cell. As the
175 LIP can be fed with intracellular and extracellular Fe sources, we compared the transcription
176 of *fbpA,* the substrate binding protein of the ferric cation ABC transporter, in WT and AitP
177 mutant exposed to sub-lethal Co^{2+} concentrations, as a proxy of extracellular Fe
178 contribution. We detected a significant increase of *fbpA* in both strains (Fig. 3D), with higher
179 levels in the AitP mutant, indicating that Fe import and probably intracellular Fe contribute
180 to Co^{2+} toxicity. Considering that the Co^{2+} sensitivity of double mutants was observed in
181 media with no added Fe (ca. 10 μM total Fe), we tested the effect of Co^{2+} on pathways
182 whose inhibition could lead to an increase in the bioavailability of iron. As Co^{2+} inhibits heme
183 synthesis and induces Fe-S disassembly, thus promoting the increase of LIP, we quantified
184 the total protoporphyrin content in both strains, exposed or not to sub-lethal Co^{2+} (Fig. 3E)
185 and measured the transcription of *sufA* in WT, a gene upregulated in response to Fe-S
186 cluster attack. Although Co^{2+} treatment decreases the level of protoporphyrin, this is similar
187 in both strains, suggesting that the Co^{2+}-mediated Fe-S cluster attack is the main
188 contributing source to LIP. Regarding this, we observed *sufA* up-regulation in WT in the
189 presence of sub-lethal Co^{2+} concentrations (Fig. 3F). We also analyzed the Co^{2+}-
190 dependency of transcriptional levels of bacterioferritin (*bfr*) and bacterioferrodoxin (*bfd*) [33],
191 as an estimate of the Fe storage status and the RirA-mediated response. Only *bfd*
192 transcription was increased by Co^{2+} (Fig. 3F). Finally, Fe-S cluster or heme synthesis

193 disruption would lead to increased Fe^{2+} bioavailability, and a suitable proxy to test this are
194 the *mbfA* and *bfr* transcriptional levels, but increases were not statistically significant (Fig.
195 1G and 3F).

196 *AitP Fe^{2+} transport likely orchestrates the initial stages of the Co^{2+}-induced Fe-S cluster*
197 *salvage pathway*

198 As Co^{2+}-dependent Fe^{2+} toxic effects seem mainly related to Fe-S clusters, the AitP function
199 may be related to driving a concerted RirA-dependent Fe-S cluster salvage/synthesis
200 pathway. If Co^{2+} accumulation led to Fe-S disassembly, we hypothesized that genes
201 regulated by RirA might be dysregulated, similarly to that observed for *fbpA* and *sufA* (Fig
202 3D and F). In particular, SMc02726 or *shmR*, a hemin-binding outer membrane receptor
203 [34], is induced in low Fe conditions and in a Δ*rirA* mutant [35]. We detected increased
204 transcripts of the outer membrane porin, ShmR, and the periplasmic component, HmuT, of
205 the ABC-heme importer HmuTUV [36](Fig. 4A). This upregulation of the heme uptake
206 system in the Ω04167 mutant suggested an exacerbated response to Co^{2+} accumulation,
207 likely due to an induced shift in the equilibrium of RirA towards the apo-form. We then tested
208 if adding hemin in the media affected the Co^{2+} sensitive phenotype detected in the Ω04167
209 strain. As shown in Fig. 4B, hemin addition to buffered TY medium (pH = 6,5) with 0.2 mM
210 Co^{2+} rescued the Co^{2+}-sensitive phenotype at concentrations between 50-200 μM. Chelation
211 of Co^{2+} by Fe-protoporphyrin IX (hemin) or metal exchange was discarded, as empty
212 protoporphyrin IX (PPIX) at 200 μM did not decrease Co^{2+} sensitivity (Fig. 4C). The detection
213 of increased transcripts of hemin transport systems in Co^{2+} treated cells led us to test the
214 hemin uptake rate under the same treatment. Surprisingly, the AitP mutant did accumulate
215 hemin at a significantly lower rate *vs.* WT (Fig. 4D and E). Although counterintuitive, this
216 result indicates that an Fe/Co-dependent post-transcriptional regulation is possible. Overall,

217 the data point to a role for AitP in Fe export under Co-rich conditions in order to concert a
218 RirA-dependent heme uptake process likely used for Fe-S cluster assembly.

219 **Discussion**

220 Cobalt is an essential element for life, and organisms like *S. meliloti* have a special
221 requirement for Co for methionine synthesis [15, 16]. However, in high concentrations it
222 proves toxic to cells. Co^{2+} efflux transporters of the CDF family have been previously
223 characterized in rhizobia, and their transcriptional regulation is mainly governed by a
224 FrmR/DmeR transcription factor [17]. Our bioinformatics analyses show that a significant
225 number of members of this family may be regulated by different factors, thus responding to
226 other effectors. Interestingly, several of these members appear under the regulation of the
227 Multiple Antibiotic Resistance Regulator (MarR) superfamily of transcription factors.
228 Although analysis of the functional roles of non-FrmR-regulated Co^{2+}-CDF is beyond the
229 scope of this work, the heterogeneity in *aitP*-like homolog regulation points to their capacity
230 to transport other divalent cations. Recent works have expanded the substrate of the Co^{2+}
231 efflux CDF transporters [7], and in this work, we have unequivocally confirmed the Fe^{2+}
232 transporting capacity of AitP by $^{59}Fe^{2+}$ transport assays in energized everted vesicles. Due
233 to the sensitivity of the mutant to high Co^{2+} but not to Fe^{2+}, from a physiological perspective
234 two questions arise: why does AitP export iron? And why is it regulated by Co^{2+}?

235 The main toxic effect of Co^{2+} in bacteria seems related to Fe-S cluster assembly [20]. In *E.*
236 *coli*, the responses to the intoxication involve the induction of the Fe-S cluster salvage
237 pathway in order to counterbalance this effect, but also, downregulation of free-Fe import
238 systems, such as Feo [23]. In contrast, *S. meliloti*, and likely all α-proteobacteria of the
239 *Rhizobiaceae* clade bearing RirA homologs, handle Co^{2+} toxicity by inducing iron uptake
240 mechanisms, i.e., triggering an Fe-starvation-like response. In *Agrobacterium tumefaciens*,
241 RirA represses genes related to free and non-free Fe uptake, and the repression is lost in

242 the presence of Co^{2+} [18]. Our results also point to an induction of the expression of these
243 iron uptake systems by Co^{2+} (*fbpA*, *shmR* and *hmuT*; Fig 3D and 4A). Similarly, this is
244 prompted by a derepression involving Co^{2+} attack on holo-RirA.

245 It has been proposed that the Fe-S cluster attack might lead to an increase of the labile-Fe
246 pool (LIP). In the presence of Co^{2+} intoxication and accumulation, the contribution of Fe from
247 the Fe-S cluster to the LIP may be detrimental by oxidative damage. We detected *suf* up-
248 regulation induced by Co^{2+}, which is in line with the increase. This could be an important Fe
249 source in low iron conditions, likely contributing to the increase in sensitivity observed in
250 double mutants lacking the main Co^{2+} efflux system and one of the Fe^{2+} exporting systems
251 (Fig 3A). As AitP-like members are also found in δ-proteobacteria, which mostly regulate Fe
252 homeostasis via direct sensing by Fur, Fe^{2+} export activity may be required to promote apo-
253 Fur and the Fe-starvation response through non-free Fe import.

254 Thus, AitP activity counterbalances the increase of LIP coming both from the release of Fe
255 from Fe-S clusters disassembled by Co^{2+} and from the Fbp-mediated entry. The latter,
256 although it represents an apparently futile Fe import-export cycle, is promoted only by Co^{2+}
257 accumulation. In agreement with our hypothesis, the addition of free iron increased Co^{2+}
258 toxicity in the AitP mutant (Fig. 3C), while the non-free iron from hemin had a protective role
259 (Fig. 4B,C), likely allowing replenishment of the intracellular pool without incurring in stress
260 for the bacteria.

261 Two more plausible, but still speculative mechanisms, involve RirA and the regulatory
262 protein, *hmuP*/*hemp* [37]. Direct attack on RirA by Co^{2+} explains the transcriptional
263 derepression observed of Fe-S cluster salvage (Fig. 3F) and hemin uptake genes (Fig 4A),
264 but still leaves the export role of Fe for AitP dispensable. A role in the fine tuning of the Co^{2+}
265 toxic response involving Fe-export by AitP might be explained considering the post-
266 transcriptional regulation of *shmR* in rhizobia [38]. A unique putative binding site for the

267 HmuP protein (a regulatory protein of *shmR*) was found in 5´UTR of *shmR* transcripts.
268 Importantly, heme binding to HmuP has been shown *in vitro* [39]. We speculate that *in vivo*
269 HmuP sensing capacity, likely via free-Fe or PPIX binding, may be involved in the post-
270 transcriptional regulation of *shmR*. Thus, a LIP increase in the AitP mutant would
271 downregulate *shmR* expression. Our data showing lower hemin uptake capacity of AitP
272 mutant *vs*. WT, even when transcripts are elevated, support this. The recovery of Co^{2+}
273 resistance in the presence of high hemin concentrations (Fig. 4B) points to an unspecific
274 uptake, or passive diffusion, mechanism in the AitP mutant. These hypotheses are currently
275 being tested.

276 Based on the above, we propose a model during Co^{2+} dyshomeostasis in which AitP would
277 detoxify both Co^{2+} and Fe^{2+}. This dual export allows cells to reduce the primary stressor
278 (Co^{2+}), while maintaining the labile-Fe pool in range despite the release of free Fe from the
279 Fe-S clusters or the entry of free Fe via ABC transporter. The lack of heme import activity,
280 even when transcripts of the importing systems are high, suggests that AitP activity is
281 involved in the orchestration of the transcription-translation process of ShmR and Hmu.
282 Future studies will focus on the role of AitP-like members in the regulation of heme uptake
283 systems and the need for other partners to achieve this regulation.

284 **Materials and methods**

285 *Bioinformatic analyses*

286 To analyze the relative abundance of the canonical "FrmR-AitP" operon architecture, *S.*
287 *meliloti* AitP (SMc04167/ SM_RS10235) homologs were searched by the best reciprocal hit
288 method [40]. Briefly, a database was created locally with all the protein sequences from
289 bacteria with a complete genome (17,972) and chromosome (2,570) assembly level
290 obtained from ftp://ftp.ncbi.nih.gov/genomes/refseq/bacteria/assembly_summary.txt
291 (August 2021). A BLAST search in this database, with WP_010969625.1 (SMc04167/

292 SM_RS10235) as query and an Expect-value of 1.10^{-5}, resulted in 13,570 subject/hits.
293 Removal of duplicated subject/hits by accession number led to 4,431 SMc04167 homolog
294 candidates. These were blasted against *S. meliloti* 1021
295 (GCF_002197445.1_ASM219744v1_protein.faa) individually. In all cases BLAST retrieved
296 WP_010969625.1 as the subject, confirming best-reciprocal-hits association. After visual
297 inspection of the subject annotations, CDFs lacking the canonical poly-histidine stretch
298 sequence (TMS4 and TMS5) were excluded in order to minimize the number of arbitrarily
299 defined "true candidates" (Expect-value<$2.19.10^{-35}$ and percentage of positive-scoring
300 matches>54%). There were 1,651 assemblies of bacterial genomes having AitP-like
301 members with unique accession numbers. This number of organisms reflects several strain
302 assemblies of the same organism, and we maintained it in order to promote the sensitivity
303 of the final assessment. These were used later to compare and create a list of 759 non-
304 redundant bacterial organisms having, or not having, the FrmR-AitP architecture. The FrmR-
305 AitP architecture search was performed using Multigenblast [41]. For these analyses, the
306 genomic database was built with approximately 4,200 genebank-formatted (.gbbf)
307 assemblies of chromosome and complete genome with identical gender and species names
308 to those drawn from the 1,651 organisms within the AitP list. The SMc04168-SMc04167
309 sequence was used to run the analyses. Results were parsed to obtain the final list of
310 organism names with the operon architecture (~500) and compared to the list of the AitP-
311 possessing organisms (~800).

312 The remaining organisms with non-FrmR-AitP-like architecture (~300) were further
313 analyzed. Three search strategies were followed to confirm the lack of FrmR(RcnR/DmeR)-
314 dependent regulation in those organisms with AitP-like members lacking the FrmR-AitP
315 architecture. In the first, the 500bp up-stream CDS region was downloaded and used in a
316 tblastn search, using the protein sequence of SMc04168/*dmeR* as query. In the second,
317 protein accession numbers of AitP-like members of this group were used to retrieve the up-

318 and downstream loci annotations, using the E-fetch “identical protein group” tool. A third
319 strategy consisted in performing a blastn search in the 500bp upstream regions for the
320 consensus FrmR consensus binding motif, using the *dmeR* binding sequence up-stream
321 SMc04167 (AAATAGGGTACCCCCCTATGCT) as query. These searches allowed us to
322 identify 27 non-FrmR-AitP-like previous candidates as false negatives, and to confirm that
323 284 AitP-like loci lack the FrmR-AitP architecture. After removal of duplicated organism
324 names, a group diagram was prepared with these numbers.

325 *Culture media, strains and mutant constructions*

326 *S. meliloti* strains (Table 1) were cultured in TY media (0.5% tryptone, 0.3% yeast extract,
327 0.09% $CaCl_2$) supplemented with streptomycin 600 µg/ml. The *S. meliloti* strain
328 Rm1021(StrR) and *E. coli* S17-1 [42] carrying the plasmid pK19mob2ΩHMB for the mutation
329 of SMc04167 were obtained from University of Freiburg, Germany (Table 1). The deletion
330 mutant strain of gene SMc04167 (Ω04167) was generated by plasmid insertion following
331 described protocols [43]. Briefly, freshly grown *S. meliloti* Rm1021 was mixed with *E. coli* S-
332 17 cells bearing the plasmid pK19mobΩHMB, containing the internal sequence of the gene
333 SMc04167, named S17-1.PI.G1PELR20F8 (www.rhizogate.de (GenDB)), and then
334 incubated overnight at 30°C on a nitrocellulose filter disk placed on LB-agar.
335 Transconjugants were recovered from the filter and selected by plating on TY-agar
336 supplemented with streptomycin 600 µg/ml and kanamycin 50–200 µg/ml. Complementation
337 was achieved by conjugation of Ω04167 with the non-integrative plasmid pJB3Tc20-P_{770}-
338 *aitP* containing gene SMc04167 plus 770 bp upstream. Transconjugants were selected on
339 TY media with kanamycin (200 µg/ml) and tetracycline (10 µg/ml). Single and double
340 mutants of *nia* (SMa1163) and *mbfA* (SMc00359) were generated by conjugation and single
341 crossover of plasmid pJQ200SK, containing a 600 bp internal region of each loci in Rm1021
342 (single mutant) or Ω04167 (double mutants). Transconjugants were selected in TY agar

343 supplemented with streptomycin 600 µg/ml and gentamycin (50 µg/ml). Mutation of *fief* was
344 performed as already described[44]. Briefly, 50 bp up- and downstream were joined to the
345 Kan^R cassette from plasmid pKD4. After purification, the fragment was introduced by
346 electroporation (1.8 kV, 600 Ω and 10 µF, 1mm gap cuvette) into BL21(DE3) cells previously
347 transformed with pKD46. In order to induce the Rec system and to increase recombination,
348 the electrocompetent cells were prepared by growing cells in LB supplemented with 1mM L-
349 (+)-arabinose at 30°C. After electroporation, cells were recovered in 5 ml of SOC media.
350 Transformants were selected in LB-agar plates with 50 µg/ml kanamycin incubated at 37°C
351 for 16 hours. Curation of the Red system was confirmed in isolated colonies that showed
352 negative growth after 16 h incubation at 37°C in LB-agar plates supplemented with 100
353 µg/ml ampicillin and 50 µg/ml kanamycin, but positive growth in plates supplemented with
354 50 µg/ml kanamycin. All strains were checked by PCR using purified genomic DNA as a
355 template and internal and external primers (Table 1).

356 *Sensitivity tests*

357 Serial dilutions of *S. meliloti* Rm1021, Ω04167, Ω00359, Ω1163, Ω03808 and Ω3004 cells,
358 initially at OD_{600nm}=0.4, were spotted (10 µl) on TY-agar supplemented with the indicated
359 transition metals (as chloride salts, except Fe^{2+} as $SO_4^{2-})^-$ or H_2O_2 concentrations for 48 h at
360 30°C. When hemin or PPIX (dissolved in 50 mM NaOH) were added to the media, the pH
361 was buffered with MES-KOH 15 mM pH 6.5, and the control conditions (0 mM hemin, 0 mM
362 PPIX) were supplemented with the same amounts of NaOH.

363 *Cobalt and iron accumulation assays*

364 Cells were incubated with 0.1 mM $CoCl_2$ for 1 hour or with 1.5 mM $FeSO_4$ in TY medium
365 during early exponential phase growth. Cells were pelleted and washed with 0.9% NaCl and
366 mineralized with HNO_3. Co or Fe were quantified by ICP-MS or Atomic absorption
367 spectroscopy.

368 *Transcriptional analyses by qRT-PCR*

369 Fold change expression levels ($2^{-\Delta\Delta Ct}$) of iron exporters and iron-related genes were assayed
370 under 20 µM, 100 µM or 200 µM $CoCl_2$, and low (0.75 mM 2,2'-bipyridyl (Bpy)), or high (0.75
371 mM $FeSO_4$) Fe^{2+} conditions *in vitro vs.* 16S reference gene. Cells were grown till the mid-
372 log phase at 30ºC in TY. After this, the culture volume was split, supplemented or not, and
373 incubated for 45 min at 30ºC before RNA extraction. Primers used are described in Table 1.

374 *Iron transport assay*

375 Fe^{2+} uptake was measured in energized everted membrane vesicles (EMV) obtained from
376 *E. coli* Δ*fieF* expressing AitP. Heterologous expression was detected by electroblotting SDS-
377 PAGE Tris-glycine gels onto nitrocellulose membranes and immunostaining with primary
378 rabbit anti-His-tag antibody and secondary goat anti-rabbit IgG phosphatase alkaline
379 conjugated antibody (GenScript, Piscataway, NJ, USA) (Suppl. Fig. 1). Vesicles were
380 obtained as previously described [45, 46] Before transport measurement, 10 µl vesicles (or
381 the equivalent to 100 µg total protein of EMV) were energized in 100 µl of transport buffer
382 (100 mM HEPES-Na, 250 mM sucrose, 50 mM KCl, 2 mM $MgCl_2$, 5 mM TCEP, pH 6.8) by
383 2-minute pre-incubation with 2.5 mM NADH at 37ºC and the uptake was initiated by addition
384 of a 10-fold concentrated $^{59}Fe^{2+}$ solution and mixing. Reaction was stopped after 5-minute
385 incubation at the same temperature by filtering through 0.22 µm nitrocellulose. Filters were
386 immediately washed with a standard solution containing 2 mM EDTA and dissolved in
387 scintillation cocktail for counting.

388 *Hemin uptake assay*

389 Hemin uptake was estimated following a previously described protocol [47]. Briefly,
390 stationary phase cells cultured in 50 ml of TY medium were incubated for 2 hours with 0.2mM
391 $CoCl_2$. Cells were centrifuged, washed once with ice-cold phosphate-buffered saline (PBS)
392 pH 7.45 and resuspended in 50 ml PBS 0.05 mM $CoCl_2$ supplemented with 30 ug/ml of a

393 hemin solution. At 2.5, 5, 15, 30, 60 and 120 minutes, one milliliter of culture was centrifuged
394 and the supernatant collected to measure the absorbance at 400 nm. No significant
395 difference was observed in the cell numbers of WT and AitP mutant strains after treatment,
396 indicating that the incubation time with Co^{2+} used does not affect cell viability.

397 *Porphyrin quantification*

398 Porphyrins were quantified following the described protocol [48]. Briefly, mid-log phase cells
399 cultured in 50 ml of TY medium were incubated for 2 hours with or without 0.2mM $CoCl_2$.
400 Cells were centrifuged, washed twice with ice-cold 50 mM Tris-HCl (pH 8.0), resuspended
401 in ethyl acetate/glacial acetic acid (3:1, v/v) to 1/100 the original culture volume, and lysed
402 by sonication on ice. Cell debris was removed by centrifugation at room temperature, and
403 the non-aqueous (top) phase was washed twice with 1 ml ddH_2O to remove residual water-
404 soluble contaminants. Extraction of porphyrins from the solution was achieved by the
405 addition of 0.5 ml 3 M HCl, and the absorbance of the bottom-aqueous phase was assessed
406 at 408 nm. Porphyrin levels were normalized to optical cell density (OD_{600nm}). No significant
407 difference was observed in the cell numbers of WT and AitP mutant strains after treatment,
408 indicating that the incubation time with Co^{2+} used does not affect cell viability.

409 **Conflict of interest statement**

410 All authors declare that research was conducted in the absence of any commercial or
411 financial relationships.

412 **Author contributions**

413 Conceived and designed the experiments: D.R., M.G.-G, I.A., P.M., T. M.

414 Analyzed the data: D.R., M.G.-G, I.A., P.M., T. M.

415 Contributed reagents/samples/analysis/tools: D.R., M.G.-G, I.A., P.M., T. M.

416 Wrote or edited the manuscript: D.R., M.G.-G, I.A., P.M., T. M.

417 All authors read and approved the final manuscript.

418 **Funding**

419 This work was supported by the Agencia Nacional de Promoción Científica y Tecnológica
420 (ANPCyT)(PICT2015-2897 and PICT2018-03139 to D.R.) and the Consejo Nacional de
421 Investigaciones Científicas y Tecnológicas (CONICET) PUE-CONICET
422 22920160100135CO. D.R. is a CONICET investigator. P.M. is recipient of a CONICET
423 doctoral fellowship. T.M. is recipient of a doctoral fellowship from ANPCyT (PICT2018-
424 03139). I.A. was recipient of a Juan de la Cierva-Formación postodoctoral fellowship from
425 Ministerio de Ciencia, Innovación y Universidades (FJCI-2017-33222).

426 **Abbreviations**

427 TM, transition metal; CDF, cation diffusion facilitator; TMS, transmembrane segment;
428 LIP, labile-Fe pool; ICP-MS, inductively coupled plasma mass spectrometry; Bpy, 2,2'-
429 bipyridyl.

430 **Acknowledgments**

431 We thank Dr. J.M Argüello for help and support on the setting of $^{59}Fe^{2+}$ transport assays.

432 **References**

433 1. Fraústo da Silva, J.J.R. and R.J.P. Williams, *The biological chemistry of the elements : the*
434 *inorganic chemistry of life*. 2nd ed. 2001, Oxford: Oxford University Press. xvii, 575 p.
435 2. Kobayashi, M. and S. Shimizu, *Cobalt proteins.* Eur J Biochem, 1999. **261**(1): p. 1-9.
436 3. Okamoto, S. and L.D. Eltis, *The biological occurrence and trafficking of cobalt.* Metallomics,
437 2011. **3**(10): p. 963-70.
438 4. Bradley, J.M., et al., *Bacterial iron detoxification at the molecular level.* J Biol Chem, 2020.
439 **295**(51): p. 17602-17623.
440 5. Pi, H. and J.D. Helmann, *Ferrous iron efflux systems in bacteria.* Metallomics, 2017. **9**(7): p.
441 840-851.
442 6. Guan, G., et al., *PfeT, a P1B4 -type ATPase, effluxes ferrous iron and protects Bacillus*
443 *subtilis against iron intoxication.* Mol Microbiol, 2015. **98**(4): p. 787-803.
444 7. Salusso, A. and D. Raimunda, *Defining the Roles of the Cation Diffusion Facilitators in*
445 *Fe(2+)/Zn(2+) Homeostasis and Establishment of Their Participation in Virulence in*
446 *Pseudomonas aeruginosa.* Front Cell Infect Microbiol, 2017. **7**: p. 84.
447 8. Abreu, I., P. Mihelj, and D. Raimunda, *Transition metal transporters in rhizobia: tuning the*
448 *inorganic micronutrient requirements to different living styles.* Metallomics, 2019. **11**(4): p.
449 735-755.
450 9. Rodionov, D.A., et al., *Computational reconstruction of iron- and manganese-responsive*
451 *transcriptional networks in alpha-proteobacteria.* PLoS Comput Biol, 2006. **2**(12): p. e163.
452 10. Hamza, I., et al., *The bacterial irr protein is required for coordination of heme biosynthesis*
453 *with iron availability.* J Biol Chem, 1998. **273**(34): p. 21669-74.
454 11. Todd, J.D., et al., *RirA, an iron-responsive regulator in the symbiotic bacterium Rhizobium*
455 *leguminosarum.* Microbiology (Reading), 2002. **148**(Pt 12): p. 4059-4071.
456 12. Bhubhanil, S., et al., *Roles of Agrobacterium tumefaciens membrane-bound ferritin (MbfA)*
457 *in iron transport and resistance to iron under acidic conditions.* Microbiology (Reading),
458 2014. **160**(Pt 5): p. 863-871.
459 13. Sankari, S. and M.R. O'Brian, *Synthetic Lethality of the bfr and mbfA Genes Reveals a*
460 *Functional Relationship between Iron Storage and Iron Export in Managing Stress*
461 *Responses in Bradyrhizobium japonicum.* PLoS One, 2016. **11**(6): p. e0157250.
462 14. Zielazinski, E.L., et al., *Sinorhizobium meliloti Nia is a P(1B-5)-ATPase expressed in the*
463 *nodule during plant symbiosis and is involved in Ni and Fe transport.* Metallomics, 2013.
464 **5**(12): p. 1614-1623.
465 15. Watson, R.J., et al., *Sinorhizobium meliloti cells require biotin and either cobalt or*
466 *methionine for growth.* Appl Environ Microbiol, 2001. **67**(8): p. 3767-70.
467 16. Cheng, J., et al., *An ABC-type cobalt transport system is essential for growth of*
468 *Sinorhizobium meliloti at trace metal concentrations.* J Bacteriol, 2011. **193**(17): p. 4405-
469 16.
470 17. Rubio-Sanz, L., et al., *Functional and expression analysis of the metal-inducible dmeRF*
471 *system from Rhizobium leguminosarum bv. viciae.* Appl Environ Microbiol, 2013. **79**(20): p.
472 6414-22.
473 18. Dokpikul, T., et al., *Regulation of the Cobalt/Nickel Efflux Operon dmeRF in Agrobacterium*
474 *tumefaciens and a Link between the Iron-Sensing Regulator RirA and Cobalt/Nickel*
475 *Resistance.* Appl Environ Microbiol, 2016. **82**(15): p. 4732-4742.
476 19. Li, Z., et al., *Nickel and cobalt resistance properties of Sinorhizobium meliloti isolated from*
477 *Medicago lupulina growing in gold mine tailing.* PeerJ, 2018. **6**: p. e5202.

478 20. Ranquet, C., et al., *Cobalt stress in Escherichia coli. The effect on the iron-sulfur proteins.* J
479 Biol Chem, 2007. **282**(42): p. 30442-51.
480 21. Thorgersen, M.P. and D.M. Downs, *Cobalt targets multiple metabolic processes in*
481 *Salmonella enterica.* J Bacteriol, 2007. **189**(21): p. 7774-81.
482 22. Macomber, L. and J.A. Imlay, *The iron-sulfur clusters of dehydratases are primary*
483 *intracellular targets of copper toxicity.* Proc Natl Acad Sci U S A, 2009. **106**(20): p. 8344-9.
484 23. Fantino, J.R., et al., *A genetic analysis of the response of Escherichia coli to cobalt stress.*
485 Environ Microbiol, 2010. **12**(10): p. 2846-57.
486 24. Chillappagari, S., et al., *Copper stress affects iron homeostasis by destabilizing iron-sulfur*
487 *cluster formation in Bacillus subtilis.* J Bacteriol, 2010. **192**(10): p. 2512-24.
488 25. Pellicer Martinez, M.T., et al., *Sensing iron availability via the fragile [4Fe-4S] cluster of the*
489 *bacterial transcriptional repressor RirA.* Chem Sci, 2017. **8**(12): p. 8451-8463.
490 26. Martinez, M.T.P., et al., *Mechanisms of iron-and O2-sensing by the [4Fe-4S] cluster of the*
491 *global iron regulator RirA.* Elife, 2019. **8**: p. e47804.
492 27. Imlay, J.A., *Pathways of oxidative damage.* Annu Rev Microbiol, 2003. **57**: p. 395-418.
493 28. Latifi, A., M. Ruiz, and C.C. Zhang, *Oxidative stress in cyanobacteria.* FEMS Microbiol Rev,
494 2009. **33**(2): p. 258-78.
495 29. Gao, F., *Iron-Sulfur Cluster Biogenesis and Iron Homeostasis in Cyanobacteria.* Front
496 Microbiol, 2020. **11**: p. 165.
497 30. Patel, S.J., et al., *Fine-tuning of Substrate Affinity Leads to Alternative Roles of*
498 *Mycobacterium tuberculosis Fe2+-ATPases.* J Biol Chem, 2016. **291**(22): p. 11529-39.
499 31. Brown, J.B., M.A. Lee, and A.T. Smith, *Ins and Outs: Recent Advancements in Membrane*
500 *Protein-Mediated Prokaryotic Ferrous Iron Transport.* Biochemistry, 2021. **60**(44): p. 3277-
501 3291.
502 32. Grass, G., et al., *FieF (YiiP) from Escherichia coli mediates decreased cellular accumulation*
503 *of iron and relieves iron stress.* Arch Microbiol, 2005. **183**(1): p. 9-18.
504 33. Costa, D., et al., *The Irr and RirA Proteins Participate in a Complex Regulatory Circuit and*
505 *Act in Concert To Modulate Bacterioferritin Expression in Ensifer meliloti 1021.* Appl
506 Environ Microbiol, 2017. **83**(16).
507 34. Amarelle, V., M.R. O'Brian, and E. Fabiano, *ShmR is essential for utilization of heme as a*
508 *nutritional iron source in Sinorhizobium meliloti.* Appl Environ Microbiol, 2008. **74**(20): p.
509 6473-5.
510 35. Chao, T.C., et al., *Role of the regulatory gene rirA in the transcriptional response of*
511 *Sinorhizobium meliloti to iron limitation.* Appl Environ Microbiol, 2005. **71**(10): p. 5969-82.
512 36. Cuiv, P.O., et al., *The hmuUV genes of Sinorhizobium meliloti 2011 encode the permease*
513 *and ATPase components of an ABC transport system for the utilization of both haem and*
514 *the hydroxamate siderophores, ferrichrome and ferrioxamine B.* Mol Microbiol, 2008.
515 **70**(5): p. 1261-73.
516 37. Amarelle, V., et al., *A new small regulatory protein, HmuP, modulates haemin acquisition*
517 *in Sinorhizobium meliloti.* Microbiology (Reading), 2010. **156**(Pt 6): p. 1873-1882.
518 38. Amarelle, V., U. Koziol, and E. Fabiano, *Highly conserved nucleotide motifs present in the*
519 *5'UTR of the heme-receptor gene shmR are required for HmuP-dependent expression of*
520 *shmR in Ensifer meliloti.* Biometals, 2019. **32**(2): p. 273-291.
521 39. Sato, T., et al., *The Small Protein HemP Is a Transcriptional Activator for the Hemin Uptake*
522 *Operon in Burkholderia multivorans ATCC 17616.* Appl Environ Microbiol, 2017. **83**(16).
523 40. Hernandez-Montes, G., J.M. Arguello, and B. Valderrama, *Evolution and diversity of*
524 *periplasmic proteins involved in copper homeostasis in gamma proteobacteria.* BMC
525 Microbiol, 2012. **12**: p. 249.

526 41. Medema, M.H., E. Takano, and R. Breitling, *Detecting sequence homology at the gene*
527 *cluster level with MultiGeneBlast.* Mol Biol Evol, 2013. **30**(5): p. 1218-23.
528 42. Simon, R., U. Priefer, and A. Puhler, *A Broad Host Range Mobilization System for In Vivo*
529 *Genetic Engineering: Transposon Mutagenesis in Gram Negative Bacteria.* Nat. Biotech.,
530 1983. **1**(9): p. 784-791.
531 43. Luo, L., et al., *Two new Sinorhizobium meliloti LysR-type transcriptional regulators required*
532 *for nodulation.* J Bacteriol, 2005. **187**(13): p. 4562-72.
533 44. Datsenko, K.A. and B.L. Wanner, *One-step inactivation of chromosomal genes in*
534 *Escherichia coli K-12 using PCR products.* Proc Natl Acad Sci U S A, 2000. **97**(12): p. 6640-5.
535 45. Gonzalez-Guerrero, M., et al., *Distinct functional roles of homologous Cu+ efflux ATPases in*
536 *Pseudomonas aeruginosa.* Mol Microbiol, 2010. **78**(5): p. 1246-58.
537 46. Raimunda, D., et al., *The transport mechanism of bacterial Cu+-ATPases: distinct efflux*
538 *rates adapted to different function.* Biometals, 2011. **24**(3): p. 467-75.
539 47. Genco, C.A., B.M. Odusanya, and G. Brown, *Binding and accumulation of hemin in*
540 *Porphyromonas gingivalis are induced by hemin.* Infect Immun, 1994. **62**(7): p. 2885-92.
541 48. Martin, J.E., et al., *The Escherichia coli small protein MntS and exporter MntP optimize the*
542 *intracellular concentration of manganese.* PLoS Genet, 2015. **11**(3): p. e1004977.
543 49. Simon, R., U. Priefer, and A. Pühler, *A broad host range mobilization system for in vivo*
544 *genetic engineering: transposon mutagenesis in gram negative bacteria.* Bio/technology,
545 1983. **1**(9): p. 784-791.
546 50. Quandt, J. and M.F. Hynes, *Versatile suicide vectors which allow direct selection for gene*
547 *replacement in gram-negative bacteria.* Gene, 1993. **127**(1): p. 15-21.
548 51. Blatny, J.M., et al., *Construction and use of a versatile set of broad-host-range cloning and*
549 *expression vectors based on the RK2 replicon.* Appl Environ Microbiol, 1997. **63**(2): p. 370-
550 9.

551 **Figures**

Figure 1.eps

Figure 2.eps

Figure 3.eps

Figure 4.eps

Table/s

552 Table 1. List of strains, plasmids and primers used in this study.

Strain/plasmid/primer

Strains	Relevant characteristics	Reference
Sinorhizobium meliloti		
Rm1021	Wild-type (Str^R)	[43]
Ω04167	Rm1021 SMc04167::pK19mob2ΩHMB- *aitP* (Str^R) (Kan^R)	This work
Ω00359	Rm 1021 SMc00359::pJQ200SK- *mbfA* (Str^R) (Gm^R)	This work
Ω1163	Rm 1021 Sma1163SMa1163::pJQ200SK- *mbfA* (Str^R) (Gm^R)	This work
Ω03808	Rm 1021 SMc04167::pK19mob2ΩHMB- *aitP*; SMc00359::pJQ200SK- *mbfA*(Str^R) (Kan^R)(Gm^R)	This work
Ω3004	Rm 1021 SMc04167::pK19mob2ΩHMB- *aitP*; Sma1163SMa1163::pJQ200SK- *mbfA*(Str^R) (Kan^R)(Gm^R)	This work
C-Ω04167	Rm 1021 SMc04167::pK19mob2ΩHMB- *aitP* / pJB3Tc20-P_{770}-*aitP* (Str^R) (Kan^R) (Tc^R)	This work
Escherichia coli		
S17-1	*E. coli 294, thi RP4-2 – Tc: :Mu-Km: :Tn7* chromosomally integrated	[49]
DH5α	F- *Φ80lacZΔM15 Δ(lacZYA-argF) U169 recA1 endA1 hsdR17 (rK–, mK+) phoA supE44 λ– thi-1 gyrA96 relA1*	Invitrogen, Carlsbad, CA, USA
BL21(DE3)pLysS	F- *ompT hsdS*B (rB-mB-) *gal dcm* (DE3) *pLysS* (Cam^R)	Invitrogen, Carlsbad, CA, USA
BL21(DE3)pKD46	F- *ompT hsdS*B (rB-mB-) *gal dcm* (DE3) *pKD46* (Amp^R)	[44]
Δ*fieF*	BL21(DE3) *fieF::Km* (Kan^R)	This work
Plasmids		
pK19mob2ΩHMB	RP4 mobilizable plasmid, Kan^R	[43]
pK19mob2ΩHMB-*aitP*	SMc04167 insertion plasmid containing a 334 bp *aitP* fragment (AL591688.1:2155814-2156147)	www.rhizogate.de
pJQ200SK	RP4 mobilizable plasmid, Gm^R	[50]
pJQ200SK- *mbfA*	SMc00359 insertion plasmid containing a 568 bp *mbfA* fragment (AL591688.1:314759-315326)	This work
pJB3Tc20	Broad host-range RK2 cloning vector, Tc^R	[51]
pJB3Tc20-P_{770}-*aitP*	SMc04167 (*aitP*) containing a 770 bp promoter fragment cloned in pJB3Tc20	This work

Primers	Sequence (5'->3')	Use
qSMc02726-ShmR-F	AGCCCAACCCTACCGATTTC	
qSMc02726-ShmR-R	CCTGTTCCGCTCTGAGATCA	
qSMc01512-hmuT-F	GTCTTCGGCGTTGGGAAATG	
qSMc01512-hmuT-R	GGTAAATGCTGGTGGAATCGCG	
qSMc1021-16S-F	GATAAGCCGAGAGGAAGGTG	
qSMc1021-16S-R	GTGTAGCCCAGCCCGTAAG	

qSMc04167-aitP-F	CGCGCTTTACCTTCGGTACG	qRT-PCR
qSMc04167-aitP-R	AATGGCCTGCGGAAAACTGA	
qSMc04168-dmeR-F	GAAAAGTTGCTCGCCCGTGT	
qSMc04168-dmeR-R	GGAGGCGACGAGGTTGAGAA	
qSMc03787-bfd-F	GGACGCCGATATATTTGATTTC	
qSMc03787-bfd-R	CGTCGCCTTTCAAGATCC	
qSMc03788-bfr-F	CGATTACGTCTCGATGAAGC	
qSMc03788-bfr-R	CTGGCCGTATTTTTCCTCAC	
qSMc00359-mbfA-F	CCTCGGAAGAGGACGATGGA	
qSMc00359-mbfA-R	GCTCTCCTCCTCCGCCATTT	
qSMc00784-fbpA-F	AACTGGTTCGGTCTGACGAC	
qSMc00784-fbpA-R	AGGCCGACATTGTAGGAGTG	
qSMc00301-sufA-F	AATATGCCGTCGATCTCGTG	
qSMc00301-sufA-R	GTCTCGAAATCCATCTGCGT	
DM-F-Sma1163-BamHI	ACTGGGATCCGACAGCACCTATGCGGCA	Cloning of 600 bp and yield of double and single mutants in *S. meliloti*
DM-R-Sma1163-XhoI	CAGTCTCGAGGTCCGTATGTCTCGCGAG	
DM-F-Smc00359-BamHI	ACTGGGATCCCTGCATGTCGCCCGTTTCG	
DM-R-Smc00359-XhoI	CAGTCTCGAGCGAGTGCCGTCATGATGC	
BamHI_AitP_-770_FW	GGGGATCCCCTCCCAGGCTAAAGCACGT	Complementation in *trans*
PstI_aitP_Stop_RV	GGCTGCAGCTCAGGCCGCCAGCGGCTCG	
Delta-fieF-F	ATGAATCAATCTTATGGACGGCTGGTCAGTCGGGCGGCGATTGCTGCGACGTGTAGGCTGGAGCTGCTTC	Generating *E. coli* Δ*fieF*
Delta-fieF-R	TTATGAAAGCATAGACCGTTTACCCTCCCTGGGTACGACGGAACAGGGGTCATATGAATATCCTCCTTAG	
Smc04167-F	AGCGAAACCCATTCACC	Transconjugant confirmation
Smc04167-R	GCCGCCAGCGGCTCGACCTC	
Smc00359-F	ATGCTCTCCCGACTTTTCTCC	
Smc00359-R	AGCATTCCCTATGACGATGCC	
Sma1163-F	TTGCGGGATATTGCGCAG	
Sma1163-R	CTCGTGCTCGAGCGATC	
up-fieF-F	CCGAACATCAGCGTCAGCA	*E. coli* Δ*fieF* confirmation
K1-R	CAGTCATAGCCGAATAGCCT	

553

Figure legends

554 **Figure 1. AitP is involved in Co^{2+}/Fe^{2+} homeostasis and the genetic context of bacterial**
555 **AitP-like transporters points to a broader transport specificity and regulation.** A)
556 Operon architecture analysis of AitP-like transporters in bacterial sequenced organisms
557 indicates the existence of a subgroup with different transcriptional regulation. B) Metal
558 toxicity was evaluated by inhibition halo assay using *S. meliloti* Rm1021 and Ω04167. Bars
559 represent the inhibition halo diameter around 7-mm filter paper discs containing 10 (black),
560 5 (dark gray), 2 (gray) or 1 (light gray) µmole of the indicated metal (as Cl^- except for $FeSO_4$).
561 Notice the Co^{2+} sensitivity in Ω04167. * = p<0.01 *vs.* Rm1021. C) Serial dilutions (10 µl) of
562 cells, initially at OD_{600nm}=0.4, were spotted on TY-agar supplemented with the indicated Co^{2+}
563 (as Cl^-) concentration for 48 h at 30°C. D) Complementation was achieved by transformation
564 of Ω04167 with pJB3Tc20-P_{770}-*aitP* (C-Ω04167 strain). Notice that Co^{2+} sensitivity was
565 restored to WT levels in the this strain. E) Cobalt (dark gray) or iron (light gray) content in
566 cells after incubation with 0.2 mM $CoCl_2$ for 1 h or 1.5 mM $FeSO_4$ for 30 min at 30°C in TY
567 medium during early exponential phase growth. Data are the mean ± SE of three
568 independent experiments. * = p< 0.05 and # = p<0.01 from a two tail Student's t-test *vs.*
569 Rm1021. F) Serial dilutions (10 µl) of cells initially at OD_{600nm}=0.4 were spotted on TY-agar
570 supplemented with the indicated hydrogen peroxide concentrations for 48 h at 30°C. G) Fold
571 change expression levels ($2^{-\Delta\Delta Ct}$ with 16S as reference gene), of *dmeR*, *aitP* and *mbfA* with
572 Co^{2+} or H) Fe^{2+} treatment with low (0.75 mM 2,2'-bipyridyl (Bpy)) or high Fe^{2+} (0.75 mM
573 $FeSO_4$). Cells were grown till mid-log phase at 30°C in TY. At this point media were
574 supplemented accordingly and incubated for 45 min at 30°C before RNA extraction. Data
575 are the mean ± SE of three independent experiments. * = p < 0.05 and # = p<0.01 from a
576 two tail Student's t-test of averaged ΔC_t (treated *vs.* non-treated/Bpy).

577 **Figure 2. AitP transports Fe with low affinity and high specificity.** Fe^{2+} uptake was
578 measured in energized everted membrane vesicles (EMV) obtained from *E. coli* Δ*fieF*

579 expressing AitP (see materials and methods). A) Time course and NADH dependency of
580 Fe^{2+} uptake into EMV. Vesicles obtained from Δ*fieF* transformed with empty plasmid (empty
581 and filled squares) or containing *aitP* (empty and filled circles) were assayed for NADH-
582 dependent Fe^{2+} uptake activity. Notice that only AitP containing EMV (filled circles) present
583 NADH-dependent activity. Initial rate conditions were assumed until 5 minutes after Fe^{2+}
584 addition. Fe^{2+} concentrations for each trace are indicated (for control conditions only 5 mM
585 traces are shown for clarity as the other concentrations did not show significant differences).
586 B) Fe^{2+} transport kinetics. Data were fitted to $v = V_{max}\,[Fe^{2+}]/\,K_{1/2} + [Fe^{2+}]$ equation by using
587 $K_{1/2}$ = 1.35±0.21 mM and V_{max} = 16.4±1.0 $nmol.mg^{-1}.min^{-1}$. C) Apparent effects on Fe^{2+}
588 transport rate by AitP of unlabeled divalent transition metals (TM^{2+}) as real substrates or
589 competitive inhibitors. Dashed line depicts the expected transport rate value obtained using
590 $v = V_{max}\,[Fe^{2+}]/\,(K_{1/2}\,(1+([TM^{2+}]/K_i))+[Fe^{2+}])$, with $[Fe^{2+}]=[TM^{2+}]=$ 2 mM and K_i assumed to be
591 equal to $K_{1/2}$. Note that only Co^{2+} affects the Fe^{2+} transport rate negatively, probably as real
592 substrate. In all cases, Fe^{2+} uptake by vesicles from empty vector-transformed strain *E. coli*
593 Δ*fieF* was subtracted prior to data analysis. In all cases, data are the mean ± SE of three
594 independent experiments.

595 **Figure 3. AitP is involved in Fe^{2+} homeostasis.** A) Serial dilutions (10 µl) of *S. meliloti*
596 Rm1021, Ω04167, Ω1163, Ω00359, Ω3004, and Ω03808 cells, initially at OD_{600nm}=0.4, were
597 spotted on TY-agar supplemented with the indicated Co^{2+} (as Cl^-) concentration for 48 h at
598 30°C. B) Cobalt content in Rm1021, Ω04167, Ω3004, and Ω03808 after incubation with 0.2
599 or 0.5 mM Co^{2+} for 1 hour at 30°C in TY medium during early exponential phase growth. C)
600 Serial dilutions (10 µl) of *S. meliloti* Rm1021, Ω04167, and C-Ω04167 cells, initially at
601 OD_{600nm}=0.4, were spotted on TY-agar supplemented with the indicated Co^{2+} (as Cl^-) and
602 Fe^{2+} (as SO_4^{2-}) concentration for 48 h at 30°C. D) Fold change expression levels ($2^{-\Delta\Delta Ct}$ with
603 16S as reference gene) of *fbpA*. Cells were grown till mid-log phase at 30°C in TY. At this
604 point media were supplemented with 200 µM $CoCl_2$ and incubated for 45 min at 30°C before

605 RNA extraction E) Total heme was estimated after cell incubation with 0.2 mM $CoCl_2$ for 2
606 hours at 30°C during the exponential growth phase. Data points and the mean of three
607 independent experiments are shown. * = p<0.05. F) Fold change expression levels ($2^{-\Delta\Delta Ct}$
608 with 16S as reference gene) of *sufA*. Cells were grown till mid-log phase at 30°C in TY. At
609 this point media were supplemented accordingly and incubated for 45 min at 30°C before
610 RNA extraction. For D) and F) Data are the mean ± SE of three independent experiments. *
611 = p<0.05 and # = p<0.01 from a two tail Student's t-test of averaged ΔC_t (treated *vs.* non-
612 treated).

613 **Figure 4. AitP activity induces heme uptake transport.** A) Fold change expression levels
614 ($2^{-\Delta\Delta Ct}$ with 16S as reference gene) of heme uptake components in WT (light gray) and
615 Ω04167 (dark gray) *in vitro vs.* 16S reference gene. Cells were grown till mid-log phase at
616 30°C in TY. After this, half of the culture volume was supplemented with $CoCl_2$ or not, and
617 incubated for 2 hours at 30°C before RNA extraction. Data are the mean ± SE of four
618 independent experiments. * = p<0.05 and # = p<0.01 from a two-tail Student's t-test of
619 averaged ΔC_t (treated *vs.* non-treated). B) Serial dilution of *S. meliloti* Rm1021, Ω04167*,*
620 and C-Ω04167 cells, initially at OD_{600nm}=0.4, were spotted (10 µl) on TY-agar supplemented
621 with the indicated Co^{2+} (as Cl^-) and hemin concentration for 48 h at 30°C. C) Serial dilutions
622 of Rm1021, Ω04167, and C-Ω04167 cells, initially at OD_{600nm}=0.4, were spotted (10 µl) on
623 TY-agar supplemented with the indicated Co^{2+} (as Cl^-) and 200 µM PPIX or 200 µM hemin
624 concentration for 48 h at 30°C. D) Hemin uptake assay of WT (light gray) and Ω04167 (dark
625 gray) cells. Different letters designate significantly different means as informed by a
626 Bonferroni post hoc (p<0.05) ANOVA test. E) Illustrative photograph of cell pellets showing
627 Co^{2+} induced hemin uptake. Cells were grown in TY at 30°C till mid-exponential phase and
628 then incubated with Co^{2+} and hemin concentrations as indicated for 2 hours (n=2). After
629 several washes, pellets were imaged. Notice the darker green color of Rm1021 cells (upper-
630 right) after the Co^{2+}+hemin incubation *vs.* Δ*aitP,* indicating increased hemin accumulation.

631 Picture shows representative results of at least three independent experiments. F)
632 Quantification of total hemin in cell pellets. *=p<0.01 vs Rm1021.

Figure 1

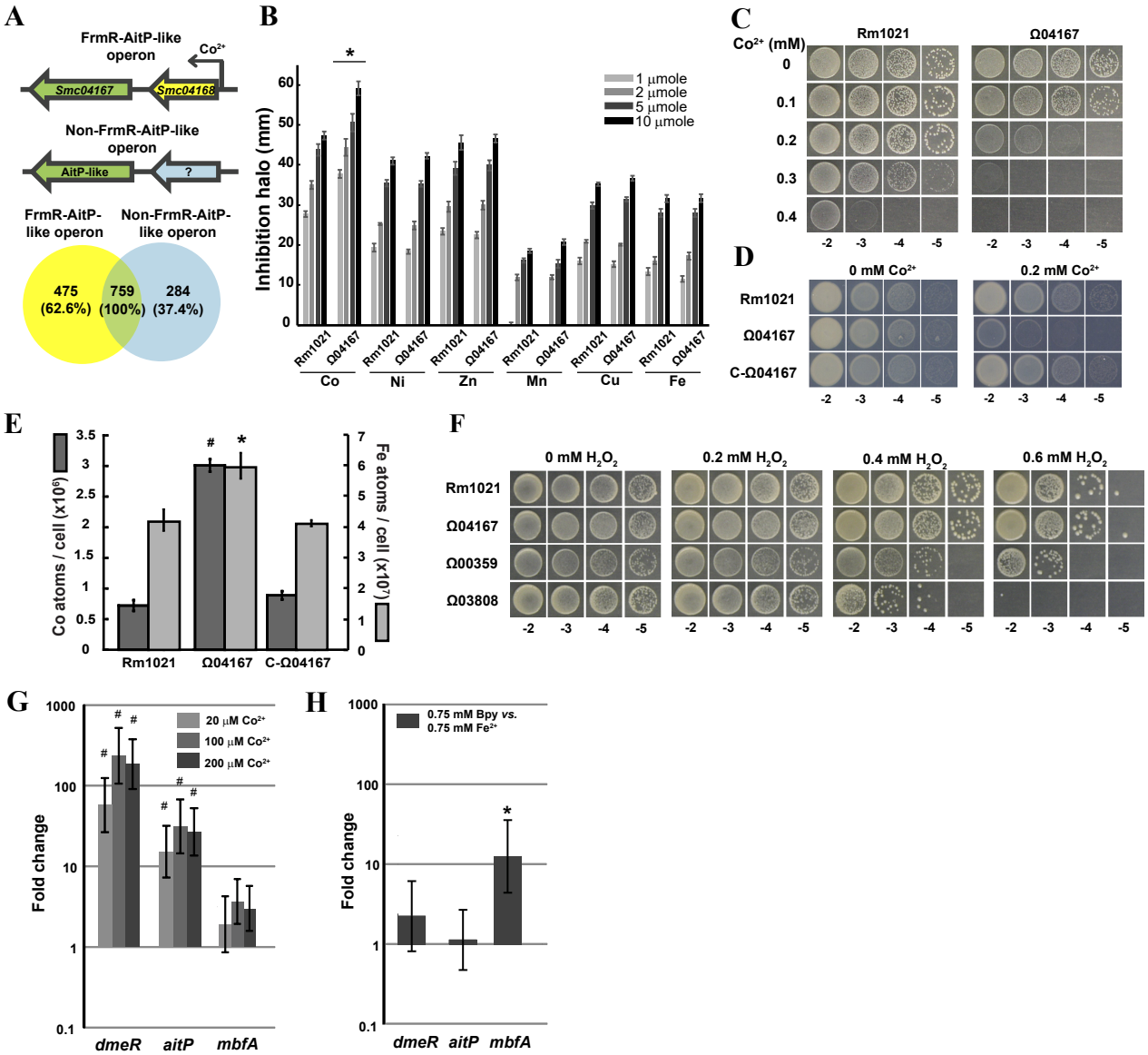
A
FrmR-AitP-like operon
Co2+
Smc04167
Smc04168
Non-FrmR-AitP-like operon
AitP-like
?
FrmR-AitP-like operon
Non-FrmR-AitP-like operon
475 (62.6%)
759 (100%)
284 (37.4%)
B
Inhibition halo (mm)
1 µmole
2 µmole
5 µmole
10 µmole
Rm1021
Ω04167
Co
Ni
Zn
Mn
Cu
Fe
C
Co2+ (mM)
Rm1021
Ω04167
0
0.1
0.2
0.3
0.4
-2 -3 -4 -5
D
0 mM Co2+
0.2 mM Co2+
Rm1021
Ω04167
C-Ω04167
E
Co atoms / cell (x10^6)
Fe atoms / cell (x10^7)
Rm1021
Ω04167
C-Ω04167
F
0 mM H2O2
0.2 mM H2O2
0.4 mM H2O2
0.6 mM H2O2
Rm1021
Ω04167
Ω00359
Ω03808
G
Fold change
20 µM Co2+
100 µM Co2+
200 µM Co2+
dmeR
aitP
mbfA
H
Fold change
0.75 mM Bpy vs. 0.75 mM Fe2+
dmeR
aitP
mbfA

Figure 2

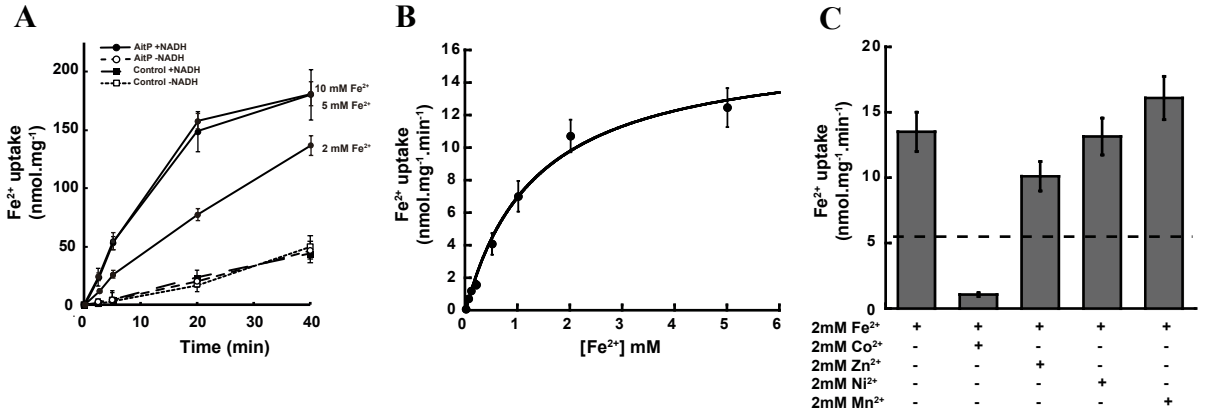
A
AitP +NADH
AitP -NADH
Control +NADH
Control -NADH
10 mM Fe2+
5 mM Fe2+
2 mM Fe2+
Fe2+ uptake (nmol.mg-1)
Time (min)
B
Fe2+ uptake (nmol.mg-1.min-1)
[Fe2+] mM
C
Fe2+ uptake (nmol.mg-1.min-1)
2mM Fe2+
2mM Co2+
2mM Zn2+
2mM Ni2+
2mM Mn2+

Figure 3

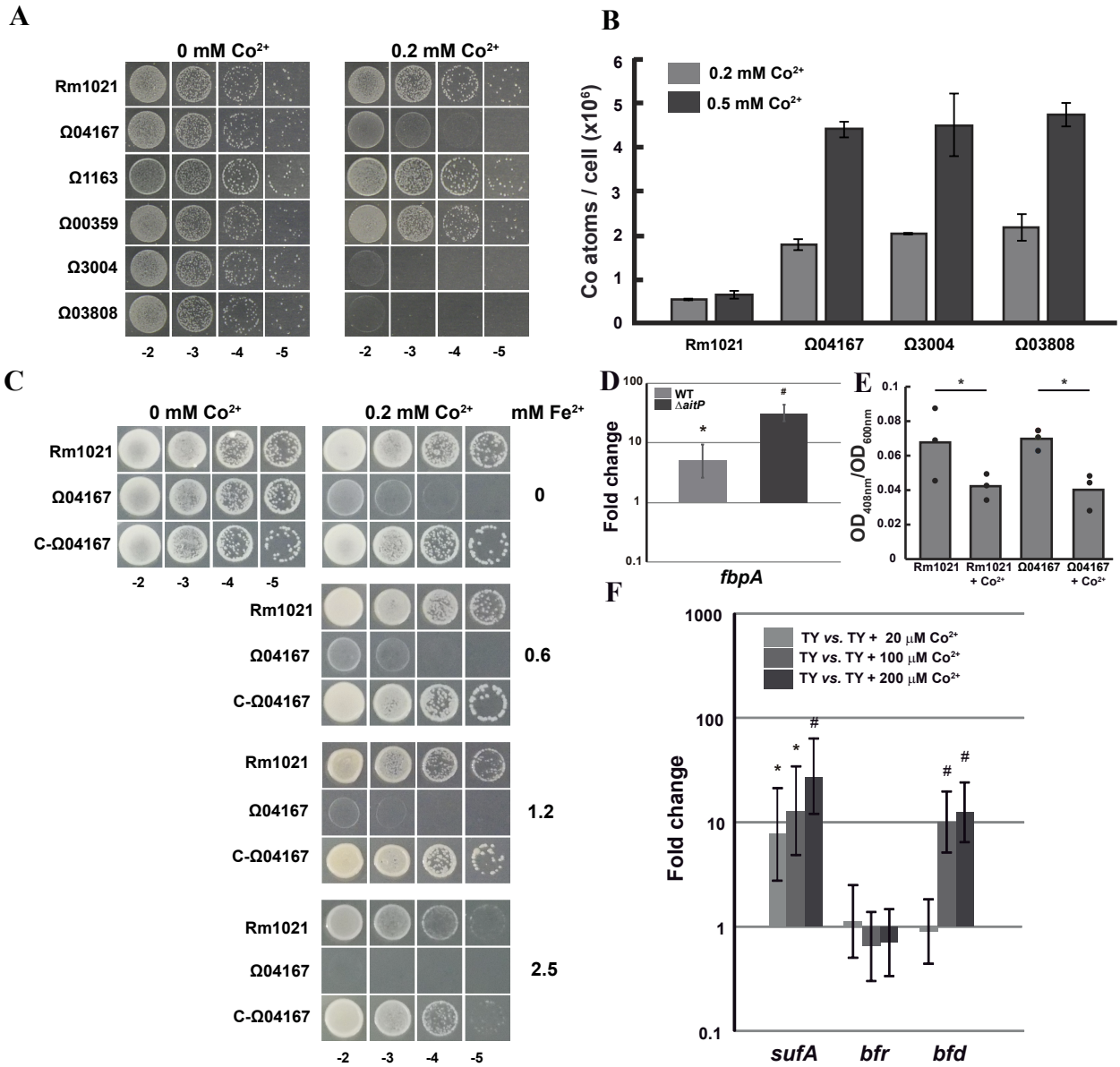
A
0 mM Co2+
0.2 mM Co2+
Rm1021
Ω04167
Ω1163
Ω00359
Ω3004
Ω03808
-2 -3 -4 -5
B
0.2 mM Co2+
0.5 mM Co2+
Co atoms / cell (x10^6)
Rm1021
Ω04167
Ω3004
Ω03808
C
0 mM Co2+
0.2 mM Co2+
mM Fe2+
Rm1021
Ω04167
C-Ω04167
0
0.6
1.2
2.5
D
WT
ΔaitP
Fold change
fbpA
E
OD408nm/OD600nm
Rm1021
Rm1021 + Co2+
Ω04167
Ω04167 + Co2+
F
TY vs. TY + 20 μM Co2+
TY vs. TY + 100 μM Co2+
TY vs. TY + 200 μM Co2+
Fold change
sufA
bfr
bfd

Figure 4

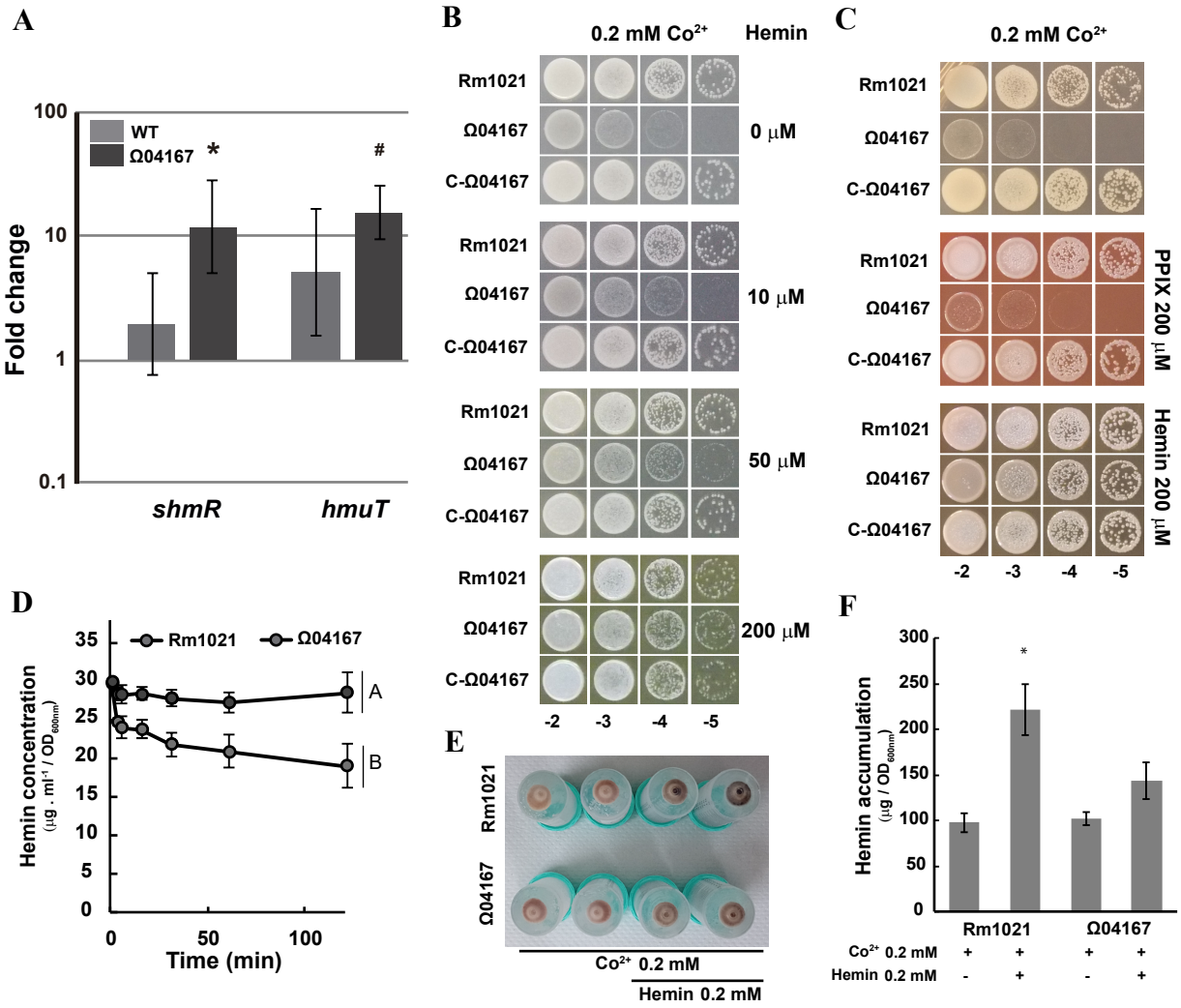
A
WT
Ω04167
*
#
Fold change
100
10
1
0.1
shmR
hmuT
B
0.2 mM Co2+
Hemin
Rm1021
Ω04167
C-Ω04167
0 μM
10 μM
50 μM
200 μM
-2
-3
-4
-5
C
0.2 mM Co2+
PPIX 200 μM
Hemin 200 μM
D
Rm1021
Ω04167
Hemin concentration
(μg . ml-1 / OD600nm)
Time (min)
A
B
E
Rm1021
Ω04167
Co2+ 0.2 mM
Hemin 0.2 mM
F
Hemin accumulation
(μg / OD600nm)
Co2+ 0.2 mM
Hemin 0.2 mM